Satellite Material Type and Phase Function Determination in Support of Orbital Debris Size Estimation

M.D. Hejduk
LZ Technologies Inc.
H.M. Cowardin
ESCG/Jacobs
E.G. Stansbery
NASA Orbital Debris Program Office

ABSTRACT

In performing debris surveys of deep-space orbital regions, the considerable volume of the area to be surveyed and the increased orbital altitude suggest optical telescopes as the most efficient survey instruments; but to proceed this way, methodologies for debris object size estimation using only optical tracking and photometric information are needed. Basic photometry theory indicates that size estimation should be possible if satellite albedo and shape are known. One method for estimating albedo is to try to determine the object's material type photometrically, as one can determine the albedos of common satellite materials in the laboratory. Examination of laboratory filter photometry (using Johnson BVRI filters) on a set of satellite material samples indicates that most material types can be separated at the 1-sigma level via B-R versus R-I color differences with a relatively small amount of required resampling, and objects that remain ambiguous can be resolved by B-R versus B-V color differences and solar radiation pressure differences. To estimate shape, a technique advanced by Hall *et al.* [1], based on phase-brightness density curves and not requiring any *a priori* knowledge of attitude, has been modified slightly to try to make it more resistant to the specular characteristics of different materials and to reduce the number of samples necessary to make robust shape determinations. Working from a gallery of idealized debris shapes, the modified technique identifies most shapes within this gallery correctly, also with a relatively small amount of resampling. These results are, of course, based on relatively small laboratory investigations and simulated data, and expanded laboratory experimentation and further investigation with *in situ* survey measurements will be required in order to assess their actual efficacy under survey conditions; but these techniques show sufficient promise to justify this next level of analysis.

1. INTRODUCTION

The characterization of orbital debris, with an eye to statistical estimation of size and therefore mass of debris collections, is one of the principal goals of the NASA Orbital Debris Program Office (ODPO). Historically, the great majority of debris survey and characterization efforts have been directed to the near-Earth (NE) orbit regime, formally defined as those objects with an orbital period less than 225 minutes; this is due to the greater satellite and debris density in the NE region and thus the greater collision hazard. Numerous formal NE orbital debris surveys have been conducted, both by regular space surveillance network radars and higher-frequency specialty radars; and the results of these surveys, together with a model that can be used to estimate object size from radar cross-section information [3], have been combined to form a quite comprehensive understanding of the NE debris environment.

With the NE debris situation reasonably well studied and understood, more attention can now be directed to the deep-space orbital debris situation (satellites with orbital periods greater than 225 minutes). Because the range-to-target of these objects is so much greater and the area to be surveyed so much larger, deep-space surveys with radar sensors are not practical. Optical telescopes thus suggest themselves as the survey instruments; and while they are better suited to tracking at greater distances (an R^2 versus an R^4 relationship) and surveying extremely broad areas, they introduce many of their own disadvantages: these sensors have less availability due to lighting and weather constraints, they can take angular measurements only, and they report an optical signature that is a function of both satellite aspect and illumination geometry (as opposed to a radar cross-section, which for monostatic radars [transmitter and receiver are collocated] is affected only by satellite aspect and not by observational configuration). Some deep-space optical debris survey work has been conducted [4, 5, 6, 7], and based on findings from the study of the NE environment certain projections about DS debris flux and density have been possible [8]; but in general it is fair to say that the DS debris situation has been only lightly investigated in comparison to the NE regime. A major

impediment to progress has been the lack of a reliable methodology for determining an estimate of an object's size from its photometric signature, as it is recognized that the common approach of presuming the object to have the shape and optical properties of a Lambertian or lunar-propertied sphere, and estimating the object's size as the diameter of such a sphere, can be no better than a first-order estimator [9]. It is the purpose of this paper to outline a survey and analysis methodology by which object size can be estimated much more robustly from optical data alone.

2. PHOTOMETRIC SIZE ESTIMATION BASICS

The illuminance ratio for a space object can be described by the following equation:

$$\frac{E_r}{E} = \frac{k\alpha A}{R^2} f(\phi) \tag{1}$$

in which k is a constant specific to the particular shape, α is the bond albedo of the object, A is the object's cross-sectional area, R is the distance from the object to the observer, and f is an attenuation function, specific to the particular shape, that is a function of the solar phase angle φ. One can reformulate the illuminance ratio in terms of stellar magnitudes through the conversion

$$\Delta_{mag} = -2.5 \log_{10}\left(\frac{E_r}{E}\right) \tag{2}$$

and create a fully serviceable relationship by fixing the sun as the illumination source

$$M_v(sat) = -26.74 + \Delta_{mag} \tag{3}$$

$$M_v(sat) = -26.74 - 2.5 \log_{10}\left(k\alpha A f(\phi)\right) + 5 \log_{10} R \tag{4}$$

When tracking an object with a telescope, one has immediate knowledge of the observed brightness M_v and potentially knows something of the color distribution of the photometric return by using either filter photometry or spectroscopy. The range-to-target R, while not directly observed, is usually also known by having tracked the object previously and performed an orbit determination (or by making presumptions about the orbit). The remaining variables in the relationship (k, α, and A), as well as the relationship $f(\varphi)$, are neither known nor directly observable; and all but one of the three must be determined in order to use (4) to solve for the remaining quantity.

This paper will propose two techniques that, taken together, show promise in being able to determine three of these four quantities, allowing the remaining variable (A) to be solved for. An approach will be outlined for using filter photometry and orbit determination to estimate material type, and with material type known one can determine the overall bond albedo α and certain key parameters of the phase function $f(\varphi)$. Additionally, an approach of examining the brightness variation distribution with phase angle will be proposed that will allow an estimation of object shape. Knowledge of the shape will permit the determination of the constant k and the functional form of the phase function $f(\varphi)$. With these parameters set, one can then solve for the cross-sectional area A; and with this and the shape known, one can calculate a characteristic size for the space object. The laboratory and simulated cases to be examined here are, of course, idealized and do not consider the additional difficulties of performing these functions with *in situ* measurements; but if they are successful in the idealized situation, they then can form a basis for additional study with extended laboratory work and preliminary survey data.

3. SATELLITE ALBEDO VIA MATERIAL TYPE AND AGOM

Determining the bond albedo of a material sample is a reasonably straightforward laboratory exercise: since the shape and area of the sample are known, a phase angle can be chosen for which $f(\varphi)$ is a known quantity (typically unity); and after measuring the illuminance ratio of the object, the only remaining unknown is the albedo (α), which can then be solved for. Additional laboratory illumination variations are required if one wishes to estimate the

proportion of diffuse to specular photometric return, but the general problem of measuring object albedo in the laboratory is not difficult. A laboratory exercise, therefore, to measure the bond albedos of common satellite materials would be straightforward, establishing a mapping between satellite material type and albedo.

Satellite characterization investigations that have attempted to estimate satellite material type have generally elected to do so with spectroscopy [10, 11], and it is not difficult to understand the reasoning: spectroscopy gives return data over a much broader range and narrowly-binned set of pass-bands, so very precise matches to candidate materials are possible due to the materials' distinctive absorption features over the broad spectral range. This more data-rich approach is, however, considerably less conducive to debris survey conditions: a minority of candidate survey instruments possess spectrometers, spectrometers are more difficult to calibrate, and the taking of even a single-observation spectroscopic dataset takes a relatively long time, thus substantially reducing the survey data throughput. While spectroscopy offers superior material properties information, its logistical and data collection burdens make it questionable for routine use in debris surveys.

Color filter photometry, however, may offer a reasonable substitute for spectroscopy, and one that is much less of an encumbrance to survey data throughput. Filter photometry has sustained multiple investigations of its ability to distinguish among closely-spaced satellites [12], to the end that special filter sets have been designed for this very application [13]. Color photometry's improved ability to distinguish among satellites is clearly related to differences in the satellites' material composition rather than satellite positioning or aspect; otherwise, similar discrimination powers would be observed using simple open-aperture photometric brightness data; but while this ability has been studied extensively *in situ*, it has resulted in relatively few published laboratory studies. The NASA OPDO Optical Measurement Center, in addition to spectroscopic measurements, has studied spacecraft materials with filter photometry using the Johnson/Bessell BVRI filters and recently published both robust average values and accompanying uncertainties for sixteen common spacecraft materials [14, 15].

Table 1: Materials investigated in the laboratory for four-color photometric response (after [14])

Reference #	Material Specimen
1	Intact MLI
2	Layer MLI - Space-facing - Copper Kapton
3	Layer MLI - Space-facing - Aluminized Kapton
4	Layer MLI - Spacecraft-facing - Copper Kapton
5	Layer MLI - Spacecraft-facing - Aluminized Kapton
6	Impacted MLI: copper kapton/mylar/beta-cloth
7	JPL Solar Panel
8	UTL Solar Cell
9	Aluminum alloy
10	Circuit board
11	Flake: Aluminum + Others
12	Potted Electronics
13	Fragmented Solar Cell
14	Glass-Fiber-Reinforced Plastic
15	Carbon-Fiber-Reinforced Plastic
16	Green Plastic Potting Material

Table 1 gives a list of the material types investigated by the study in [14], along with a reference number that will appear in certain figures to follow. Some of the material specimens are near-pristine spacecraft samples from the original manufacturers, and others derive from satellite fragmentation experiments and thus represent partial, fragmented, and/or pitted exemplars. The investigation determined that the color-difference paradigm that was most revealing was a B-R / R-I comparison, and this is what is shown on the left side of Fig. 1 for the first twelve of the sixteen materials examined, with the right side giving the 1-σ measurement uncertainty boxes about each point. Because the uncertainty correlation between the two datasets (covariance) is not known, the uncertainty areas are represented as simple uncertainty (Bonferroni) boxes. As one can see, there is quite a bit of overlap among many, indeed most, of the boxes, leading one to question whether these different materials can truly be separated based on color photometry alone.
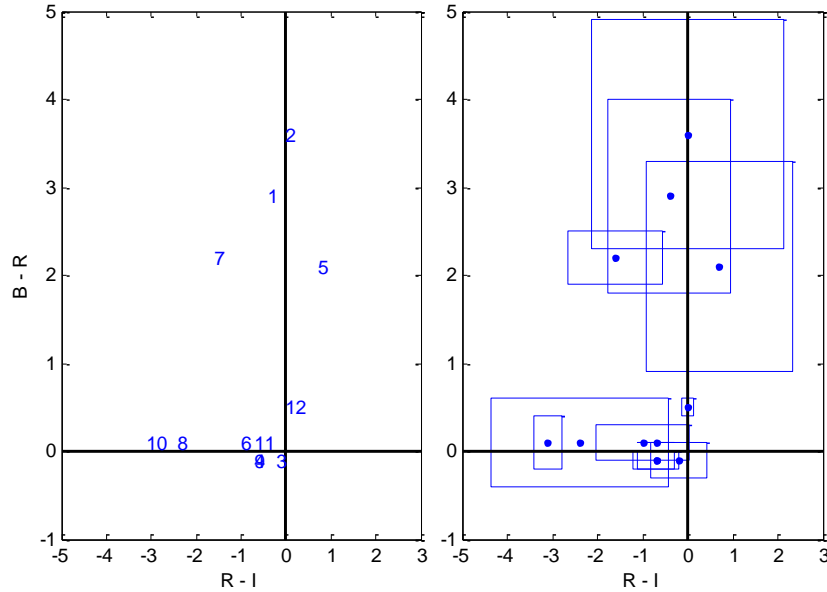
Fig. 1: Color-difference plot, with and without uncertainty, for 12 of the 16 study materials

It is important to realize, however, that these 1-σ uncertainties apply only to the estimation of the mean from a single sample; if multiple samples (meaning multiple observations) are obtained and the mean or median estimated from these multiple samples, then the estimation uncertainty is reduced. To determine how much multiple sampling will reduce these uncertainties, the following resampling investigation was performed. One hundred thousand 2, 3, 5, and 10-point samples of each of the R-I and B-R measurements were produced, using the original mean and standard deviation from the laboratory measurements as seed data for the random number generation. In each case, the median value was estimated from the 2, 3, 5, and 10-point samples, and the 68th percentile of these estimates was taken as a non-parametric proxy for a 1-σ value. These synthetic 1-σ values were then used to draw the modified uncertainty regions shown in Fig. 2. As one can see, using just two samples instead of one shrinks the uncertainty areas substantially; and using five samples produces physical separation of nearly all the uncertainty areas. A ten-sample approach produces a separation in every case (except for materials 4 and 9, located in the bottom-right part of the left side of Fig. 1, which overlap completely; a different technique for separating these materials will be proposed shortly). This approach does impose the survey requirement of multiple sampling of individual objects, and therefore the necessity of performing a state estimate in order to make possible subsequent follow-up; but it does appear that with this increased sampling color photometry has the potential to effect material type identification reliably.

Four of the sixteen materials were omitted from the above analysis because they produced so faint a return in I-band that an R-I value could not be calculated. While it is not the most robust of procedures, it does seem reasonable to use the circumstance of a low-I-band return as a separation mechanism for placing these four material types in their own separate class, to be further separated by a different color indexing procedure. Fig. 3 shows these four materials (numbers 14 and 15 are completely superimposed) on a B-R / B-V color-difference graph on the left side and the associated uncertainty areas on the right. Fig. 4 shows these same areas with median estimates from two and five sample resampling, respectively; even the two-sample resampling adequately separates those materials that actually have non-identical medians, with the five-sample resampling making the separation that much stronger.
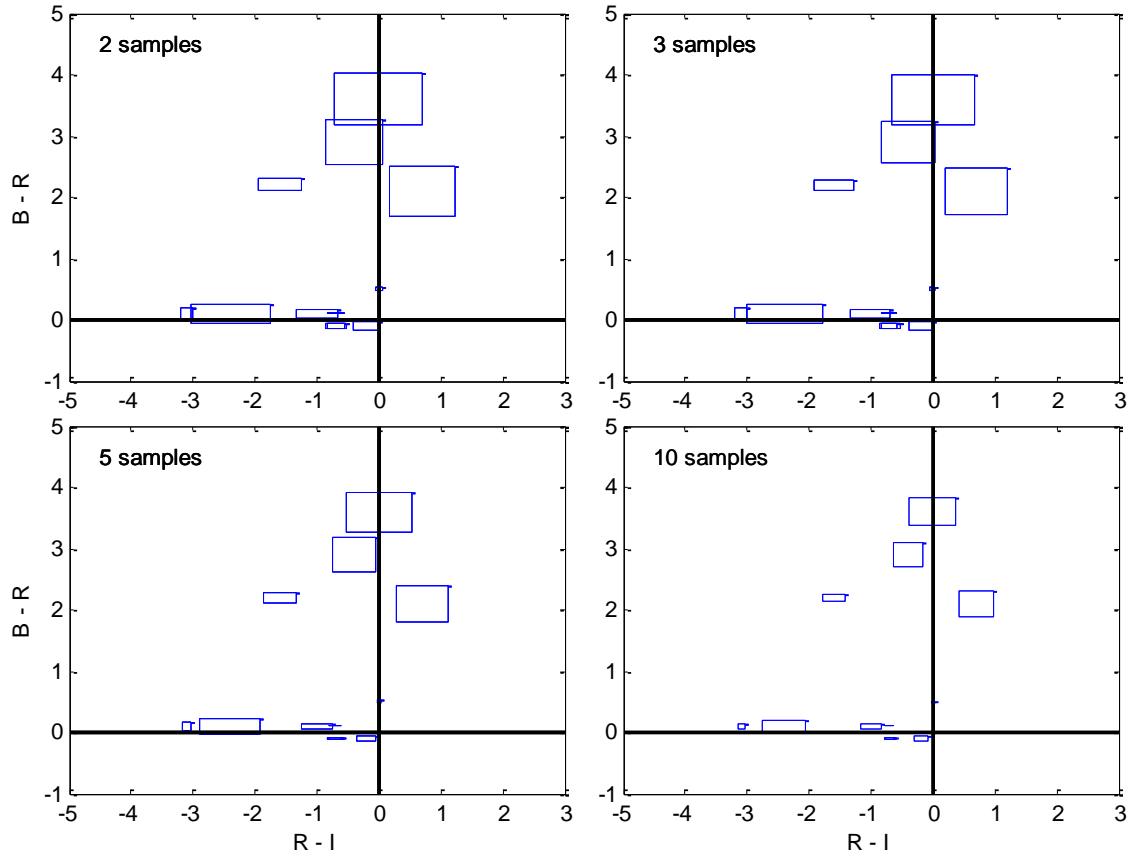
Fig. 2: Change in color-difference uncertainty volumes with number of samples
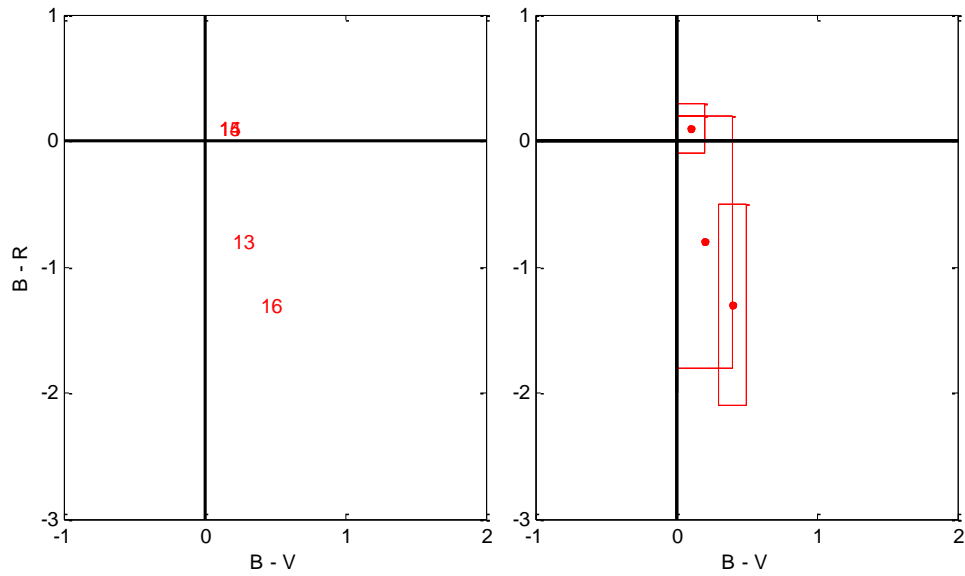

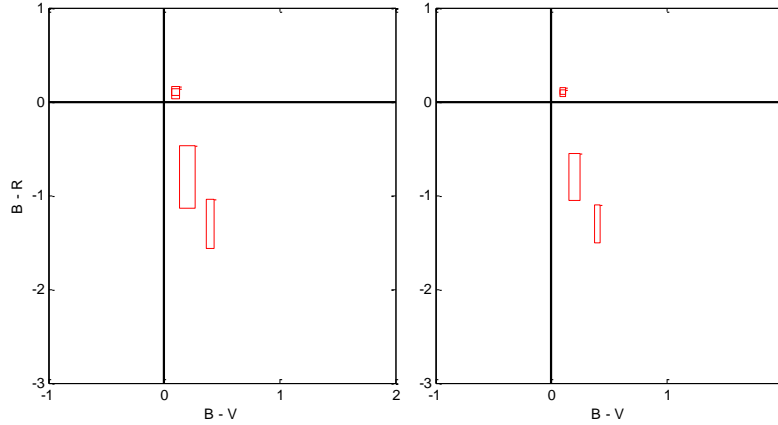**Fig. 3: Color-difference plot for four materials with low I-band returns**

Fig. 4: Change in color-difference uncertainty volumes with number of samples for materials with low I-band returns

At this point, two pairs of materials were not successfully separated by these two different color comparisons: materials 4 and 9 from Fig. 1 (MLI versus solar cell fragment) and materials 14 and 15 from Fig. 3 (circuit board versus aluminum flake). Fortunately, there is a third technique available: the use of a solar radiation pressure solution to estimate the area-to-mass ratio of the object. Solar radiation pressure is the non-conservative force resulting from the momentum that the sun's illumination imparts to the spacecraft, the resulting acceleration of which is given by the following relationship [16]

$$\ddot{r} = -P_s C_R \frac{A}{M} \frac{\vec{r}_s}{r_s^3} \ , \tag{5}$$

in which P_s is the solar radiation pressure in the vicinity of the Earth (usually in units of watts-seconds per cubic meter), C_R is the radiation pressure coefficient (which essentially defines the absorptivity of the satellite's construction materials), A is the effective area of the satellite's surface exposed to the solar radiation, M is the spacecraft's mass, r_s is the distance to the sun, and $\vec{r}_s$ is the unit vector from the satellite to the sun. In examining this equation, one can see in the grouping of C_R, A, and M a similar construct to the ballistic coefficient; because in the first treatments of the subject [17] the symbol used to represent C_R was the Greek letter γ, this ballistic-coefficient-like quantity is called AGOM (Area-[times]-Gamma-Over-Mass). This quantity is an estimated parameter in most high-fidelity orbit determination algorithms. If multiple revisits of the object (on the order of five) are already required, and if these revisits will span more than one observing session, then a durable estimate of AGOM from the OD process is a reasonable expectation. This procedure does not estimate the area-to-mass ratio *per se*; but since the constant C_R almost always has a value between 1 and 2 [16], one can expect AGOM to serve as a proxy for area-to-mass ratio at least within that fidelity. This level of accuracy is likely to be adequate to the task, as the dynamic range of the AGOM values associated with common satellite materials can be quite large. AGOM values for solid, dense objects, such as rocket bodies and intact payloads, are typically in the 0.01-0.03 range [18], values for MLI are often observed to be in the 1-20 range [19], and intermediate materials can be expected to occupy values perhaps in the vicinity of 0.1. Certain object types, such as those with high area-to-mass ratios, can manifest fluctuating and highly variable AGOM values; but it is expected that with modest resampling a reasonable mean value can be computed and used for comparisons.

With this expected performance, AGOM can be used to separate the two sets of material pairs that could not be distinguished by color photometry alone. The first set, numbers 4 and 9, constitutes a piece of MLI and piece of solar cell; the MLI fragment should have an AGOM value greater than 1, and the solar cell fragment should have an AGOM value in the same range as that for a payload, certainly less than 0.1; there should thus be an order of magnitude difference between the two AGOM values, making them easily distinguishable. The second set, numbers 14 and 15, constitutes a circuit board and an aluminum flake. The circuit board should have an AGOM value in the 0.1 range or less, whereas the aluminum flake should have a value much closer to that for the lower end of MLI.

While this latter example is less clear-cut, there still should be enough separation between the two values to allow separate classification.

Of course, these results represent the idealized case of examining satellite materials in the laboratory. While some of the material samples were from actual fragmentation experiments, others were manufacturers' pristine material coupons; and all of them were evaluated in a sea-level laboratory rather than a vacuum environment emulating the actual environment in which such fragments would be observed. These laboratory results thus neglect the "space reddening" effect in which object colors shift further to the red as time on orbit increases, believed to be due to the leaching of atomic oxygen due to the space vacuum. While some preliminary work has been performed to try to characterize this time-varying behavior [20], considerable additional study is needed to produce a color transformation function that will allow an equivalence to be established between laboratory and in situ measurements. The present investigation does, however, suggest that this general approach of determining material type through color photometric measurements is indeed viable, thus motivating the additional study required to develop the needed color transformation function.

4. SHAPE INFORMATION

In order the better to understand the production and composition of space debris, a number of laboratory satellite collision experiments have been conducted, in which an intact spacecraft is intentionally kinetically destroyed and the produced fragments collected and characterized. These experiments have included the SOCIT 4 destruction of a completed Transit satellite bus [21], six microsatellite fragmentations conducted by Kyushiu University [22], and a rocket body explosion staged by the European Space Operations Center (ESOC). The JSC/ODPO has either sponsored these experiments directly or has collaboratively arranged for the resulting fragments to be examined and catalogued.

The analysis of these satellite fragments gives some idea of the different fragment shapes that are likely to compose the debris population. The shape analysis of the SOCIT 4 experiment was the most regularized, producing a helpful analysis of shape composition by fragment size: "nuggets" (pitted ellipsoids) predominate from the smallest sizes up to 4mm; "flakes" (facets with often one bent or curled edge) constitute the majority from 4mm to about 2cm, and above this size the "other" category is used to encapsulate cubes, rectangular prisms, cylinders, spheroids, &c. Given the capabilities of the optical instruments likely to be available for deep-space debris surveys, it is unlikely that they will be able to characterize, let alone track, objects smaller than 5cm and probably not much smaller than 10cm; so such surveys are likely mostly to encounter the "other" shape categories, which were not catalogued expansively in [21] due to that experiment's focus on the smaller objects. The investigations in [23] and informal surveys of the fragmentation objects in residence at the ODPO indicate that objects > 5cm in size can be reasonably assigned to the following shape categories: 1) facets, which can include rectangular prisms; 2) cylinders, both squat and elongated; 3) spheroids or "globs," which can be ellipsoidal but lean towards the spheroidical; and 4) needles/wires. This latter category will need more investigation in the laboratory to determine the best modeling approach (long, thin cylinder; long, thin rectangular prism; specular reflector only); but for the present exploration of shape determination, the following shapes have been chosen: two-sided facet, rectangular prism (which, in its 1x1x1 state, includes the cube), cylinder (both snub and elongated), and icosahedron (as a representative spheroid.).

5. SHAPE DETERMINATION

Determining object shape from photometric response has typically been performed with light curves—long telescopic dwells (often tens of minutes to hours) on single objects in order to characterize the change in photometric intensity with time [24]. This technique promises perhaps the most exact solutions, as light curves bear a large amount of data; but their interpretation is exceedingly complex, often intuitive, and not well suited to deterministic solution, especially for precessing objects. Some work has been done on constructing physical models to predict the expected attitude of debris objects [25], and when this research has come fully to fruition it may reduce the complexity of the light-curve interpretation problem; but for the present it is prudent to examine techniques that make use of point photometry, as this may obviate the difficulties of light-curve interpretation and additionally afford more survey flexibility.

The most promising of such techniques is that of Hall *et al.* [1], who recommend examining data-density plots of an object's brightness as a function of solar phase angle: in such plots the x-axis is the solar phase angle, the y-axis is the object's brightness, and the out-of-plane dimension (here rendered as a color in a color-intensity plot) is the data density, or number of measurements with a particular phase angle – brightness ordered pair. The key insights that engendered this technique are 1) that the brightness versus phase density would have a distinctive

appearance based on object shape and independent of attitude and 2) the dimmer portion of the density plot would additionally be distinctive and, because it is the dim portion, would be largely to entirely free of influence by the specular response of the object—thus eliminating the need to make an estimate of object material type. The analysis thus required a paradigm for matching an object's actual observed photometric response density to those for various shapes simulated via Monte Carlo techniques. Hall *et al.* proposed for this a Kolmogorov-Smirnov approach adapted to matching two-dimensional distributions and demonstrated its effectiveness against a reasonably data-rich set of photometric measurements of a NE satellite.

Fig. 5 shows these photometric measurement density plots for the shapes called out in Section 4 above, using an 80% diffuse / 20% specular photometric mixture and the Cook-Torrance specular response model for a gold metal material type (a "middle-of-the-road" material for specular response and thus a reasonable choice for a general investigation [26]). Ten thousand randomly-selected sun and observer vectors were chosen for each 1-degree bin in phase angle, producing 1.8 million Monte Carlo pairs of vectors with a uniform distribution in phase. The diffuse response alone is shown in the first box of each vertical set, then the specular response alone below that, and then the combination of both in the final frame. The colors indicate the logarithm of the density of the measurements, with black/blue indicating the lowest densities and red the highest. The white line at the bottom of the diffuse response curve represents a curve-fitting approach that attempts to detect the "ragged edge" of the dim response and then fits a polynomial to this edge, with the winning polynomial fit (up to degree 15) determined by the lowest Akaike Information Criterion (AIC) score [27], an information theory technique commonly used to evaluate model fitting of data.

Hall *et al.* developed this overall technique for the purposes of satellite characterization; and thus they could legitimately confine themselves to a circumscribed number of shapes that were well approximated by Platonic solids. The present project is interested in estimating debris object size and therefore must consider alterations to the basic shapes that would affect a size measurement, such as the growing of a cube into an elongated rectangular prism and the growing of a "squat" 1x1 cylinder (height equal to diameter) into an elongated cylinder. Additionally, given that the material types of debris objects are likely to vary substantially, it would be helpful to adapt any shape-recovery technique so as not to require knowledge of material type, either *a priori* or through observation.

To achieve this, one approach has been to try to use the dim edge of the brightness density, represented by the white lines shown in Fig. 5, to identify the particular shape. What is particularly attractive about this approach is that, since it operates off of the dim edge of the brightness density, it can be expected to be largely unaffected by specular response and thus material type. These "white line" curve fits do produce different behaviors for some of the shapes, such as for the two-sided facet and for the icosahedron; but in other cases they are identical: the curves for the snub and oblong cylinders, cube, and rectangular prism are essentially indistinguishable. Furthermore, while some objects have a reasonably distinct definition of the dim edge up to a certain phase angle (such as the cube up to 90 degrees in phase and the icosahedron up to about 150 degrees), other shapes, such as the two-sided facet and the cone (not shown here explicitly), have a ragged edge over the whole of phase space and thus will require a large amount of sampling to try to determine that edge definition robustly. As such, the approach of fitting the dim end of the brightness response is not an immediately promising candidate for the shape-separation needs of the present problem.

The Hall *et al.* study's preliminary trials confined themselves to a single material type and thus executed the two-dimensional Kolmogorov-Smirnov distribution comparison technique with this particular variable fixed. To see whether this assumption can be generally applied—namely, whether the specular effects of different materials are similar enough that, for the purposes of shape determination, they can be treated as essentially constant—the calculations used to produce Fig. 5 were re-run for a single shape (1x1x5 rectangular prism) and ten different material types. There is no known reliable, comprehensive BRDF database of spacecraft materials, so ten material types not dissimilar to spacecraft materials and their Cook-Torrance BRDF parameters were taken from the MIT BRDF materials database [26], a rigorously-produced repository of BRDF measurement information. Table 2 enumerates the particular materials chosen, and Fig. 6 gives three illustrative examples of the different results. The left column of Fig. 6, representing silicon nitride, shows a very weak specular response that essentially leaves the diffuse brightness completely unmodified. The center column, representing metallic blue, shows a stronger specular response than the metallic gold used in the initial shape survey of Fig. 5; but while it does alter the overall response somewhat from the pure diffuse component, the summed diffuse/specular response still has the overall look-and-feel of the diffuse response. The right column, representing polyurethane, has an extremely broad-lobed specular component that produces a summed result that is different from the diffuse response alone—mostly increasing the frequency of brightness measurements in the "diffuse" brightness region rather than producing canonical bright speculars. This is a varied set of responses that, in at least some cases, can affect the results in the diffuse region; so

it is important to select a shape determination approach that will behave robustly in the face of broadly different types of specular response.
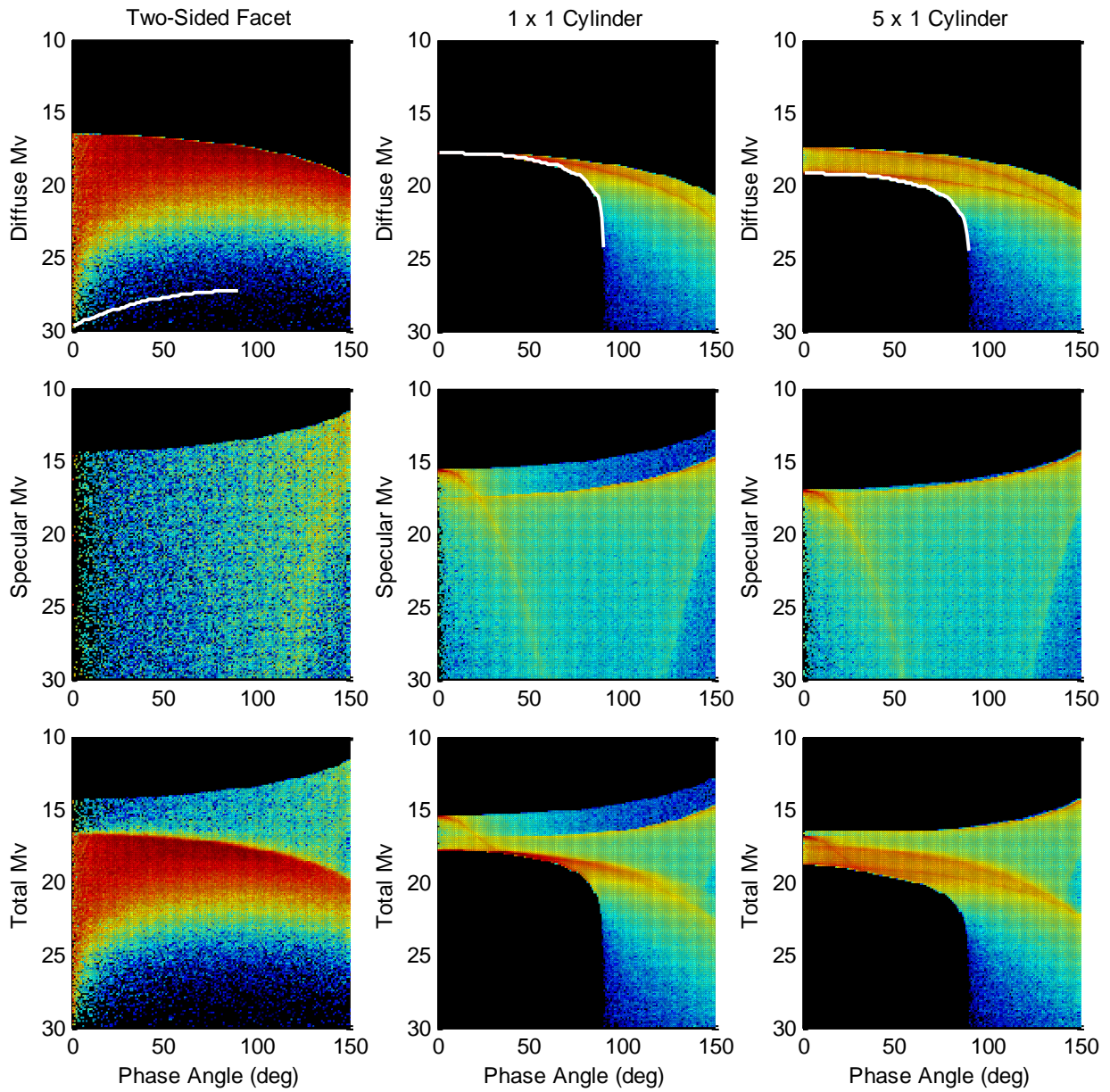

Fig. 5a: Brightness vs phase intensity plots for the two-sided facet and two cylinder types
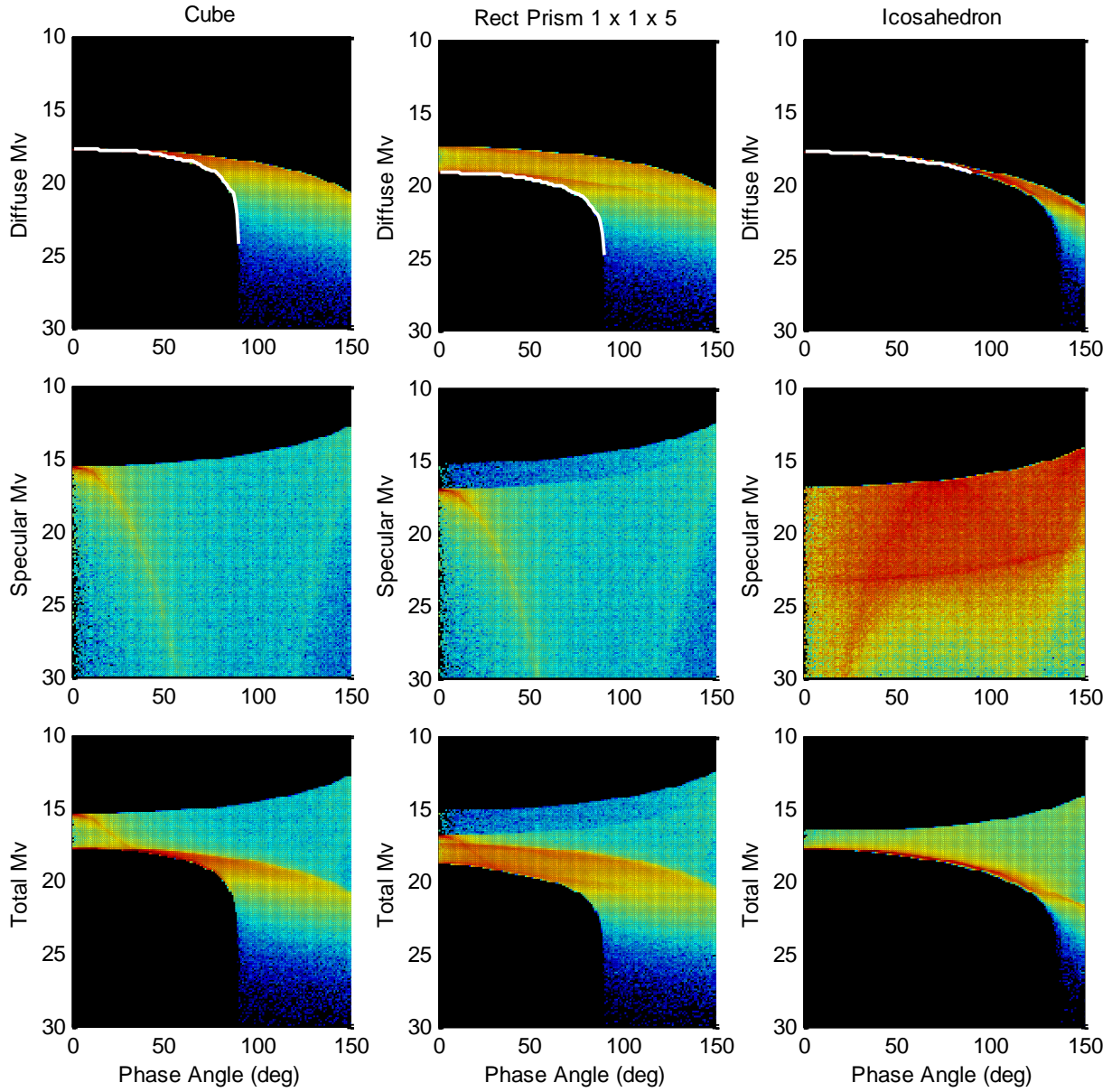
Fig. 5b: Brightness vs phase intensity plots for the cube, elongated rectangular prism, and icosahedron

Table 2: Material types investigated for specular response-

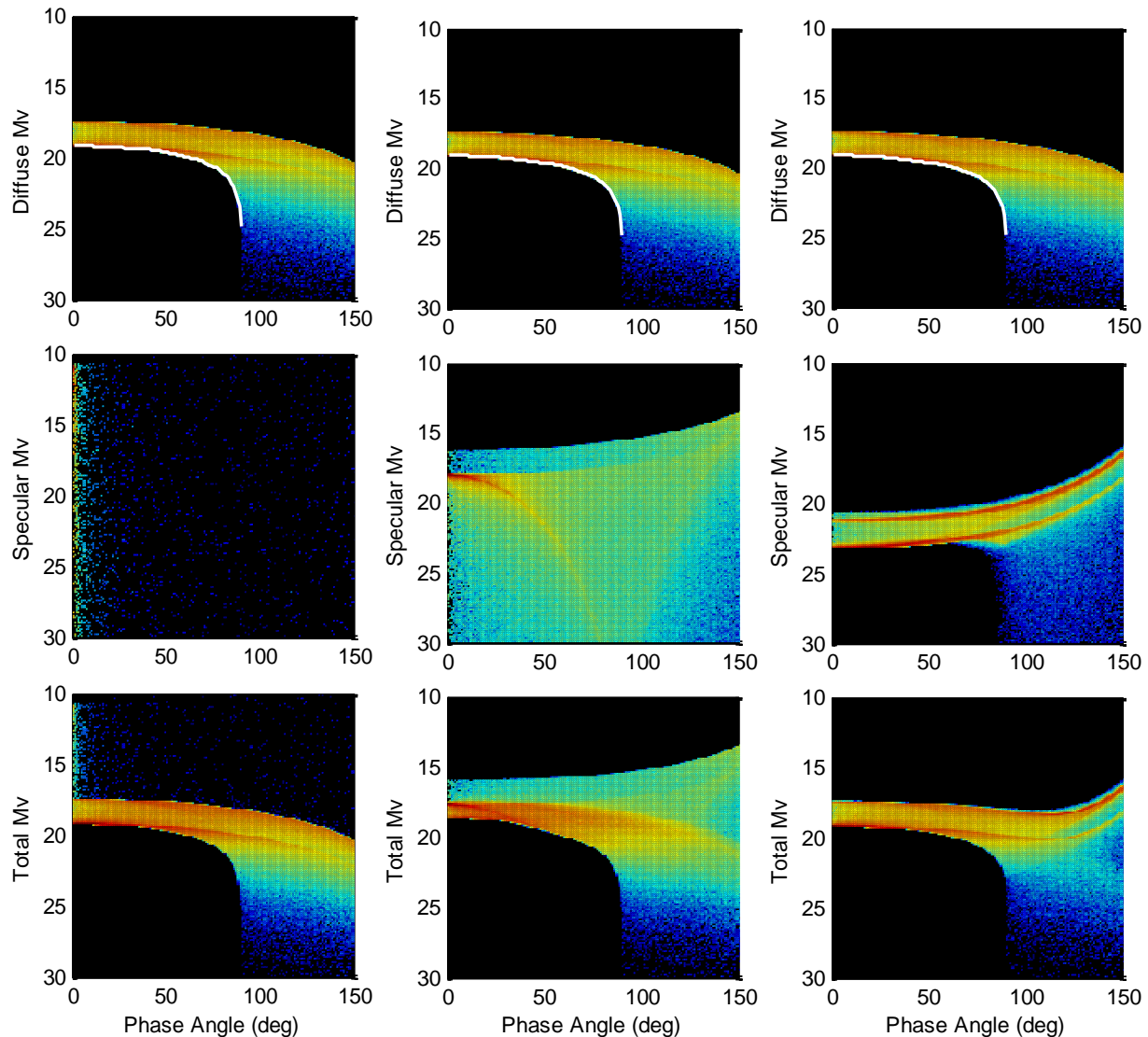| #	Material	#	Material
1	Metallic Gold	6	Delrin Plastic
2	Aluminum Bronze	7	Metallic Blue
3	Aluminum	8	Polypropylene
4	Copper	9	Polyurethane
5	Black Plastic	10	Silicon Nitride

Fig. 6: 1x5 rectangular prism with three very different material properties (left column to right column): silicon nitride, metallic blue plastic, and polyurethane

One way in which this might be done is to examine a relatively narrow band of phase angles, chosen perhaps in a region of the phase-brightness intensity plot that is somewhat less perturbed by changes in the material properties and subsequent differences in specular reflection. If response within this band can be considered essentially uniform with phase angle, then the distribution to analyze can be reduced from two dimensions (the whole of the brightness-phase density plot) to one dimension (the response in just this band). There are many more statistical techniques available for analyzing and comparing one-dimensional distributions (essentially histogram analysis); so this reduction in dimensionality, while it does in a way exclude much of the brightness information from the shape-assignment analysis, allows more and varied statistical tools to be brought to the investigation.

The logical approach with which to begin is cumulative distribution function (CDF) analysis; essentially the integral of a histogram, a CDF is the usual way that histogram information for different distributions is compared, and it eliminates the arbitrariness of histogram bin definition. Comparison of CDFs should give a more manageable and, if desired, quantifiable difference set between the distributions for different material types. In
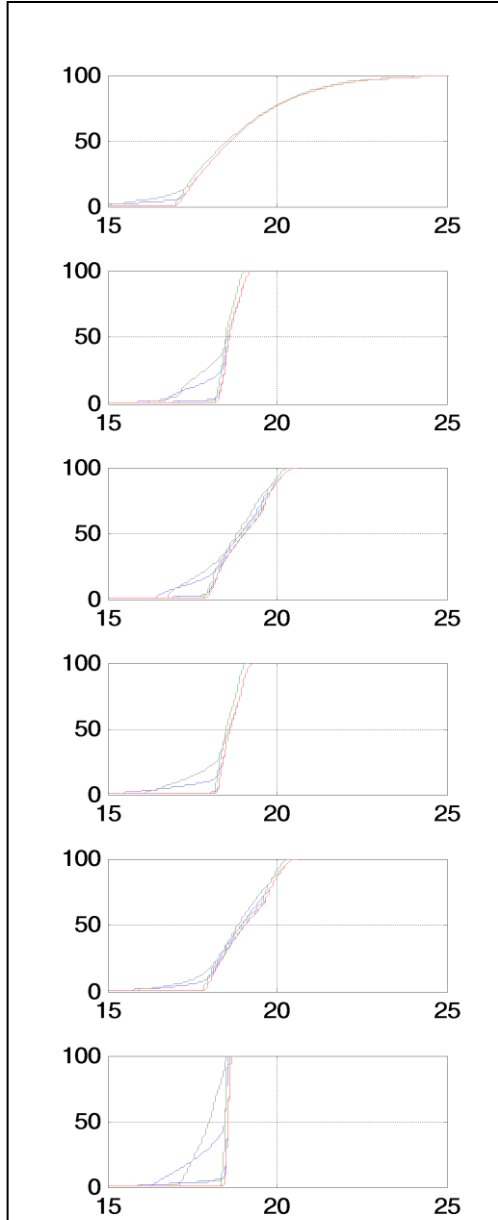
Fig.7: CDF plots of brightness distributions in 70-75 degree bin for the six shapes used in this study (facet, 1x1 and 1x5 cylinder, cube, 1x1x5 rectangular prism, and icosahedron). Brightness (in stellar magnitudes) is given on x-axis; cumulative percentage on y-axis.

examining the plots of Fig. 5, a good candidate for a phase angle wedge seems to be the band of 70 to 75 degrees, so the photometry for each of the ten different material types modeled for each shape was extracted for that phase angle band and formulated into a CDF, the results of which are presented in Fig. 7. Each of the six plots maps to one of the shapes in the usual order of this paper (two-sided facet, 1x1 cylinder, 5x1 cylinder, cube, 1x1x5 rectangular prism, and icosahedron), and each of the CDF lines within each plot corresponds to one of the ten material types investigated. In these plots, the x-axis gives photometric brightness in M_v and the y-axis cumulative percentage.

These plots possess several interesting features, the amalgamation of which leads to a promising discrimination technique. First, it is noticed that, while there can be substantial variation in the CDF plots below about the 40th percentile point on the CDFs, above this point there is a substantial convergence of the ten CDF curves; for the icosahedron the convergence is more frayed, but it is strong for the other shape types. So it would seem that this region of the distribution—greater than the 40th percentile (which is the dimmer side)—exhibits behavior that is mostly independent of material type. Second, the portion of the CDF between the 40th and 80th percentiles very much approximates a straight line (a bit of a stretch for the two-sided facet, but still the behavior is not particularly curved), and the slopes of these "linear" portions appear to vary with shape. To ensure that this is not simply a *trompe l'œil* of the presentation, the data from this percentile region were extracted for each shape-material pair, ordinary least squares was used to fit a line to these data, and the slopes of these lines for the ten material types were averaged for each shape. The results of these calculations are given in Table 3. One can observe very large slope differences between shapes that have been seen to have very different photometric responses and smaller differences between those that have been seen to be similar (*e.g.,* 5x1 cylinder and 1x1x5 rectangular prism). These slopes are a good mechanism to distinguish among the five shapes, with the possible exception of distinguishing between the elongated cylinder and rectangular prism.

Table 3: CDF middle-part slopes associated with different shapes

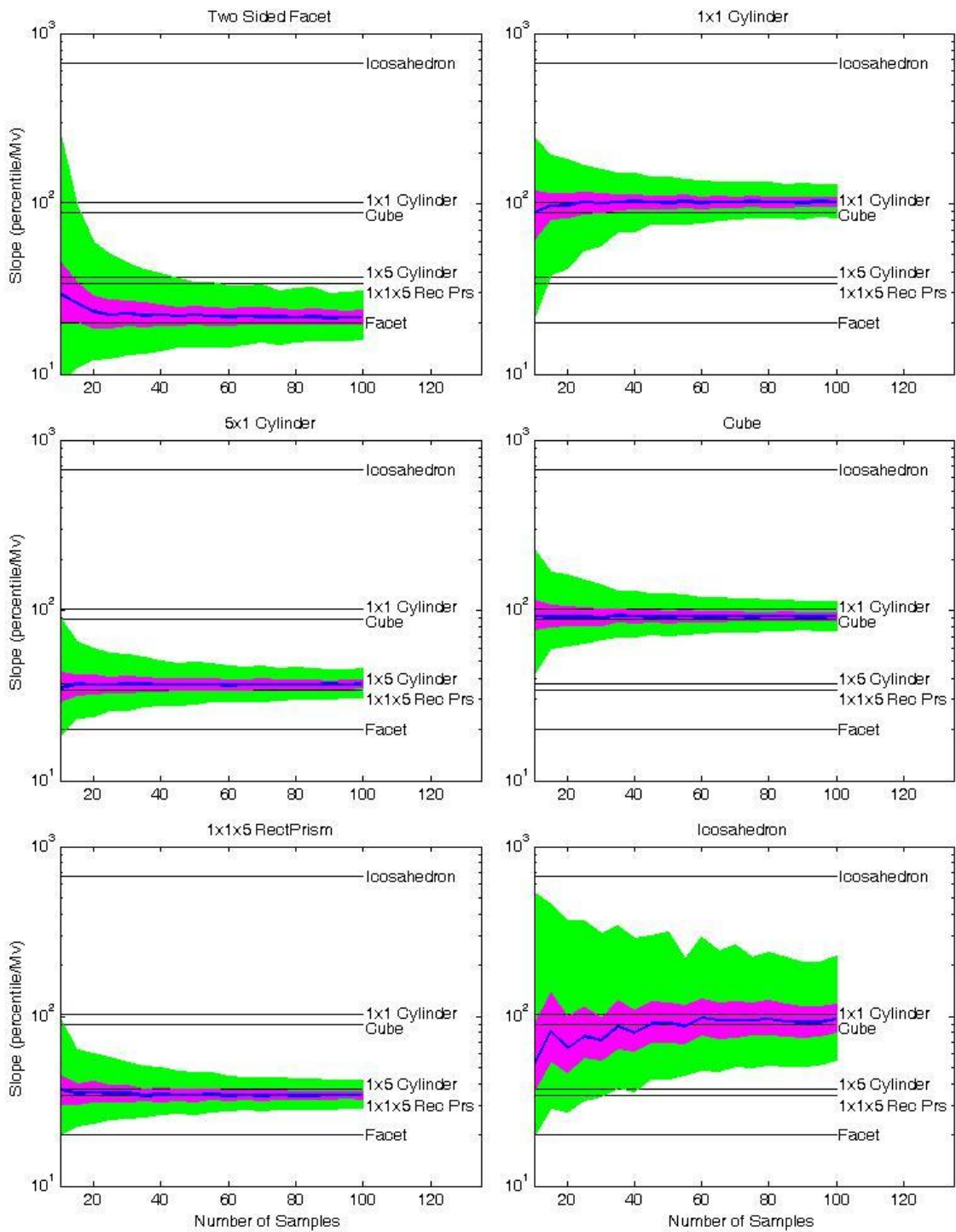| Shape Type	Average Slope of 40 - 80 Percentile
Two-sided Facet	20.07
1x1 Cylinder	102.22
5x1 Cylinder	36.91
Cube	89.03
1x1x5 Rectangular Prism	34.07
Icosahedron	666.95

Fig. 8: Resampling error regions for estimating CDF slope from limited sampling

The operative question, of course, is the number of samples required to calculate such a slope with any reliability; to determine this, a resampling technique similar to that for the color photometry uncertainty evaluation in Section 3 was employed. Using the Monte Carlo photometry points for each shape, one thousand sets of 10 samples, 15 samples, 20 samples, &c. up to 100 samples were drawn; and all of these groups of one thousand

samples were described by the 5th, 32nd, 50th, 68th, and 95th percentiles. These percentile values can be used to approximate 1-sigma and 2-sigma uncertainty regions about the estimated 50th percentile (a proxy for the mean) as a function of sample size. The estimated slope data from Table 3 are combined with these median estimate and uncertainty region results and given in Fig. 8. In this figure, the estimated slope data from Table 3 are shown as horizontal lines, each labeled with the shape to which they correspond. The estimation results are shown as envelope regions about the estimated median; the 1-sigma proxy is given in magenta and the extension to a 2-sigma proxy in green. The propriety of the technique is thus determined by how well, and with what degree of sampling, the sampling estimate from a shape's Monte Carlo photometry converges on the actual averaged CDF slope for that shape.

One can see that the results are extremely encouraging overall. With one exception, all shapes are properly identified within a 1-sigma uncertainty with fewer than 20 samples, and a 2-sigma uncertainty with fewer than 40 samples. These resampling requirements strike the authors as reasonably low and certainly within the capabilities of debris survey conditions. With additional sampling, the technique can differentiate between the narrowly-differentiated shape types of rectangular prism and cylinder (*i.e.,* squat cylinder and cube, and elongated cylinder and elongated rectangular prism), but never within a 1-sigma uncertainty. Since these shape-type pairs are essentially identical from the point of view of object size estimation, that a shape identification approach would confuse them is not of particular significance, as they would render essentially the same size estimates. The icosahedron is the lone exception—not only is it not properly identified by the technique, it is actually misidentified as a squat cylinder or cube. From a size estimation perspective, this would not be a death-dealing misidentification, as the induced error in the size estimation would be relatively small; but it is a misidentification nonetheless. Proper identification of this shape type may require some additional data-taking, such as some tracking at a relatively large phase angle (*e.g.,* 110 degrees or so) to determine whether a ragged edge or clear density at that point is observed, since the icosahedron will manifest a grouped density with a similar dim point to the 70-75 degree density, as opposed to a "ragged edge" situation for the cube. Of course, if the detections are already at the dim edges of the instruments' capabilities because the object is so dim, it may not be possible to perform this additional experiment; so it may be desirable to develop a more robust discrimination technique for the icosahedron case.

Despite the promise shown for this technique, one must not become prematurely sanguine about its ease of implementation. The number of different shapes and material types examined were relatively small; so the immediate next step in its development is to expand the gallery of shapes and material types to see whether discrimination is as strong and clear among larger groups of both. After this, laboratory verification is needed: shape models with different materials need to be constructed and observed in the laboratory and the technique deployed (and refined) against these measurements. Finally, telescope observations of objects with a known shape need to be obtained and submitted to this technique to determine how well it functions with actual telescopic data. Only at this point would the technique be ready to serve as an integral part of a debris survey.

6. SURVEY CONDUCT AND PREPARATORY WORK

If both of the techniques described above (material type determination through color photometry and shape identification through phase-versus-brightness data density examination) were fully vetted, how might a deep-space debris survey be conducted the best to make use of them? It would seem that the contemporaneous use of two different types of instruments, or perhaps the same instrument in two different modes, would constitute the most efficient procedure. A large-throughput searching sensor, such as the recently-constructed DARPA-sponsored Space Surveillance Telescope (SST), can conduct searches of orbital regions of interest multiple times per night, taking both optical metric data and open-aperture photometry. If multiple observations are acquired each evening, and especially if a "spiraling" search methodology is employed that revisits each initial search frames on the order of a few minutes after the initial exposure, orbit determination should be possible with the angles-only observations, which should allow proper association of future observations with their brethren. As the amount of data increases and thus produces enough open-aperture photometry to perform shape estimation, a parallel effort can be conducted to collect enough filter photometry on this object to estimate material type. When enough data have been collected to allow both shape and material estimation, the satellite can be placed in an inactive maintenance status—serendipitous observations from the continuing survey should be sufficient to maintain the object and therefore ensure that objects acquired in the future are not confused with this object. This seems a straightforward procedure that would both establish a dim-object DS catalogue and provide object size estimates needed to feed debris models.

7. REFERENCES

1. Hall, D., Calef, B., Knox, K., Bolden, M. and Kervin, P. "Separating Attitude and Shape Effects for Non-Resolvable Objects." 2007 AMOS Technical Conference, Kihei, HI. September 2007.
2. Kessler, D.J, Johnson, N.L., Liou, J.-C., and Matney, M. "The Kessler Sydrome: Implications to Future Space Operations." *Advances in the Astronautical Sciences*, ed. S.C. McQuerry, vol. 137, 2010.
3. Lambour, R. *et al.* "Assessment of Orbital Debris Size Estimation from Radar Cross-Section Measurements." *Advances in Space Research* 34 (2004), pp. 1013-1020.
4. Potter, A. and Mulrooney, M. "Liquid Metal Mirror for Optical Measurements of Orbital Debris." *Advances in Space Research* 19 (1997), pp.213-219.
5. Abercromby, K. *et al.* "A summary of Five Years of Michigan Orbital Debris Survey Telescope (MODEST) Data." 59th International Astronautical Congress. Glasgow, Scotland. September-October 2008.
6. Abercromby, K. *et al.* "The Geosynchronous Earth Orbit Environment as Determined by the CCD Debris Telescope Observations between 1998 and 2002: Final Report." February 2008, NASA/TP-2008-214774.
7. Abercromby, K. *et al.* "Michigan Orbital Debris Survey Telescope Observations of the Geosynchronous Orbital Debris Environment, Observing Years: 2007-2009." September 2011, NASA/TP-2011-217350.
8. Mulrooney, M.K., Matney, M.J., Hejduk, M.D., and Barker, E.S. "An Investigation of Global Albedo Values." 2008 AMOS Technical Conference, Kihei, HI. September 2008.
9. Hejduk, M.D. "Phase Functions of Deep-Space Orbital Debris." 2007 AMOS Technical Conference, Kihei, HI. September 2007.
10. Jorgensen, K. "Using Reflectance Spectroscopy to Determine Material Type of Orbital Debris." Ph. D. thesis, University of Colorado, Boulder, May 2000.
11. Bédard, D. "Using a Physics-based Reflection Model to Study the Reddening Effect Observed in Spectrometric Measurements of Artificial Space Objects." 2011 AMOS Technical Conference, Kihei, HI, 2011.
12. Payne, T.E., and Gregory, S.A. "Passive Radiometric Observations of Geosynchronous Satellites." *Proceedings of the IEEE*, 2004.
13. Payne, T.E., Gregory, S.A., Sanchez, D.A., Burdullis, T.W., and Storm, S.L. "Color photometry of geosynchronous satellites using the SILC filters." Proc. SPIE 4490, 194 (2001).
14. Cowardin, H.M. "Characterization of Orbital Debris Objects over Optical Wavelengths via Laboratory Measurements." Ph.D. thesis, University of Houston, Clear Lake, May 2010.
15. Cowardin, H., Seitzer, P., Abercromby, K., Barker, E., and Schildknecht, K. "Characterization of Orbital Debris Photometric Properties derived from Laboratory-based Measurements." 2010 AMOS Technical Conference, Maui, HI.
16. Montenbruck, O. and Gill, E. *Satellite Orbits: Models, Methods, and Applications.* Berlin: Springer Verlag, 2000.
17. Koskela, P. E. "Orbital Effects of Solar Radiation Pressure on an Earth Satellite." *The Journal of the Astronautical Sciences*, IX, 3, 1962.
18. Hejduk, M.D. and Ghrist, R.W. "Solar Radiation Pressure Binning for the Geosynchronous Orbit." 2011 AAS Astrodynamics Specialists Conference, Girdwood, AK. August 2011.
19. Kelecy, T. Payne, T., Thurston, R., and Stansbery, G. "Solar Radiation Pressure Estimation and Analysis of a GEO Class of High Area-to-Mass Ratio Debris Objects."
20. Abercromby, K. *et al.* "Remote and Ground Truth Spectral Measurement Comparisons of FORMOSAT III." 2007 AMOS Technical Conference, Maui, HI.
21. Krisko, P.H., Hortsman, M. and Fudge, M.L. "SOCIT4 Collisional-breakup Test Data Analysis with Shape and Materials Characterization." Advances in Space Research 41 (2008), pp. 1138-1146.
22. Hanada, T., Liou, J.C.,Nakajima, T., and Stansbery, E. "Outcome of Recent Satellite Impact Experiments." *Advances in Space Research* 44, 4 May 2009.
23. Cowardin, H. *et al.* "Characterization of Orbital Debris Photometric Properties derived from Laboratory-based Measurements." 2011 AMOS Technical Conference, Maui, HI.
24. Lambert, J.V. *et al.* "Photometric and Spectral Analysis of MPC Object J003E3." *Proceedings of the IEEE* (2004), Vol. 5, pp. 2866-2873.
25. Ojakangas, G.W. and Hill, N. "Toward Realistic Dynamics of Rotating Orbital Debris and Implications for Light Curve Interpretation." 2011 AMOS Technical Conference, Kihei, HI, September 2011.
26. Matusik, W., Pfister, H., Brand, M., and McMillan, L. "A Data-Driven Reflectance Model." *ACM Transactions on Graphics* 22, vol 3 (2003), 759-769.
27. Akaike, Hirotugo. "A New Look at the Statistical Model Identification." IEEE Transactions on Automatic Control 19 (1974), vol. 6, 716-723.